arXiv:1512.05487v1 [astro-ph.SR] 17 Dec 2015

Hypergiant V1302 Aql in 2001–2014

V.G. Klochkova,[1⋆], E.L. Chentsov,[1] A.S. Miroshnichenko,[2] V.E. Panchuk,[1] and M.V. Yushkin[1]

[1] – Special Astrophysical Observatory RAS, Nizhnij Arkhyz, 369167 Russia
[2] – Department of Physics and Astronomy, University of North Carolina at Greensboro, Greensboro, NC 27402–6170, U.S.A.

December 18, 2015

Abstract We present the results of a study of spectral features and the velocity field in the atmosphere and the circumstellar envelope of the hypergiant V1302 Aql, the optical counterpart of the IR source IRC+10420, based on high-resolution spectroscopic observations obtained in 2001–2014. We measured radial velocities of the following types of lines: forbidden and permitted pure emissions, absorption and emission components of lines of ions, pure absorptions (e.g., He I, Si II), and interstellar components of the Na I D–lines, K I, and DIBs. The heliocentric radial velocity measured for pure absorptions as well as for the forbidden and permitted pure emissions is close to the systemic radial velocity and equal to $V_r = 63.7\pm0.3$, 65.2 ± 0.3, and 62.0 ± 0.4 km s^{-1}, respectively. Positions of the absorption components of the lines with inverse P Cyg profiles are stable and indicate the presence of clumps moving toward the star with a velocity of $\sim$20 km s^{-1}. The average radial velocity of the DIBs is $V_r(\mathrm{DIB}) = 4.6\pm0.2$ km s^{-1}. Comparison of the absorption lines observed in 2001–2014 and those in earlier data shows no noticeable variations. We conclude that the hypergiant reached a phase of slowing down (or termination) of the effective temperature growth and is currently located near the high-temperature boundary of the Yellow Void in the Hertszprung-Russell diagramme.

Key words. stars: massive, supergiants – techniques: spectroscopic – stars: individual: V1302 Aql

1. Introduction

The evolutionary status of a very luminous star V1302 Aql, the optical counterpart of the IR source IRC+10420, has been unclear. The variety of its properties allowed to classify it either as a Proto-Planetary Nebulae (PPN) [1] or as a very massive star that has passed through the red supergiant phase [2]. PPNe are currently thought to be low-mass peculiar supergiants with strong IR excesses in a short-term transition from the Asymptotic Giant Branch to the Planetary Nebula (PN) stage. They are descendants of intermediate-mass stars (initial masses 1–8 $M_\odot$) which have passed several evolutionary stages, including switching energy sources and stages with typical mass loss rates up to $10^{-5}\,M_\odot\,yr^{-1}$ and even up to $10^{-4}\,M_\odot\,yr^{-1}$. As a result, a PPN is a low-mass degenerate C–O core surrounded by a tenuous and usually an asymmetric envelope. As the core contracts, its effective temperature (T_{eff}) rises and the star moves blueward in the Hertsprung-Russell diagramme (hereafter HRD). This stage may last until T_{eff} reaches $\sim$30000 K, when ionisation of the circumstellar envelope begins. At this time, the object is observed as a PN after hydrogen recombination lines and forbidden lines of light elements show up in its spectrum. Luminosity of low-mass supergiants at the PPN stage may reach $\log L/L_\odot \sim 4.5$ [3].

Yellow supergiants are significantly different from PPNe, although a number of properties (high luminosity, spectral features, presence of circumstellar envelopes) are similar in these two classes of object. Predecessors of the former are massive (initial mass $\geq 20\ M_\odot$) and the most luminous stars,

⋆ E-mail: valenta@sao.ru

which lose a significant part of their mass after leaving main-sequence, become red supergiants, and later proceed to yellow supergiants. A typical luminosity of a yellow supergiant is $\log L/L_\odot \sim 5.3$–5.9 [2]. These objects are located near the Eddington limit in an instability region which contains hypergiants of spectral types from A to M [4, 5]. Wolf-Rayet stars and Luminous Blue Variables may be their descendants [6]. Structured circumstellar envelopes of hypergiants formed during several phases of a strong stellar wind with mass loss rates of $10^{-4} - 10^{-3}$ $M_\odot\,yr^{-1}$ are sources of IR and maser radiation as well as of numerous molecular emission lines. Nevertheless, the yellow hypergiant ρ Cas, nearest to V1302 Aql in HRD and possessing an extended and unstable atmosphere [7], shows no signs of circumstellar material [8].

Obviously, depending on the adopted nature and hence luminosity of an object, its distance estimate may differ by a factor of a few. However, data obtained during the last two decades from various observations leave no doubts that V1302 Aql is an object at the yellow hypergiant stage (see review by Oudmaijer *et al.* [6]) as well as later papers [9, 10]. Moreover, V1302 Aql is now considered to be the most unambiguous massive Galactic object with a highest mass loss rate which undergoes a short-term evolutionary transition from a red supergiant to a Wolf-Rayet star [11]. One of the most compelling arguments confirming its high-luminosity massive star status has been derived from spectroscopic data obtained at the 6 m telescope of the Russian Academy of Sciences, when the authors [12] found a significant nitrogen excess in the atmosphere of V1302 Aql. In all the spectra obtained between 1997 and 2000, a He I 5876 Å lines with a large equivalent width of $\geq$200 mÅ was detected. With the object's T_{eff} ~9200 K, such an equivalent width can be a consequence of a high luminosity and an enhanced helium abundance in its atmosphere [13, 14].

Interest to V1302 Aql has been growing in the last decade due to detection of a 120 K a year T_{eff} increase [12, 14, 15, 16] that allowed to suggest evolution toward the Wolf-Rayet stage. Humphreys *et al.* [17] points out that V1302 Aql is a post red supergiant star which is crossing a critical HRD region called the Yellow Void [18].

The T_{eff} increase stimulates us to continue spectroscopic monitoring of this mysterious object. High-resolution spectroscopy is required to refine the structure and kinematics of its circumstellar envelope. The most adequate model to represent the observed kinematics is, in our opinion, the "rain" model proposed by Humphreys *et al.* [17] even considering a bipolar model suggested later [10]. Observations with a moderate spectral resolving power, $R \sim 8000$, were obtained by Humphreys *et al.* [17] to test the model. We obtained spectra with a much higher resolution (up to $R \sim 60000$) that allows us to better constrain the line profiles and measure their parameters with a much higher accuracy.

In this paper, we present the results of a new stage of a spectroscopic monitoring of V1302 Aql in continuation of our study of this object [12, 14]. In Section 2 we describe our spectroscopic data, Section 3 is devoted to discussion of the results, while Section 6 summarizes the conclusions.

2. Observational Data

We have added 16 new spectra to our collection of the V1302 Aql data in 2001–2014. The observing dates and data spectral ranges are listed in the first two columns of Table 1. Most spectra were obtained with the échelle spectrograph NES with spectral resolution $R = 60000$ [19, 20]. Our first spectrum obtained on 2001 August 9 was taken with the spectrograph LYNX 1K×1K CCD, $R \sim 25000$ [21]. One-dimensional data were extracted from 2D échelle spectra using the *ECHELLE* context in *MIDAS* modified to features of the spectrographs used (see details in [22]). Cosmic particles were removed by median averaging of two consecutive spectra. Wavelength calibration of the spectra was derived using a Th-Ar hollow cathode lamp.

One of the spectra used in this paper was obtained at the McDonald Observatory on 2009 September 11 with the échelle spectrograph TS2 $R = 60000$ [23] in the coudé focus of the 2.7 m Harlan J. Smith telescope. This allowed us to fill the gap in observations with the 6 m telescope for 2009. One-dimensional data for this spectrum were extracted using the *apall* task within the *echelle* package in IRAF. In particular, the spectral range of this observation allowed us to study profiles of the strong lines of Ca II 8408 Å and 8542 Å in the near IR region, which is not covered by the 6 m telescope data.

Table 1. Averaged heliocentric velocities for groups of lines in the spectra of V1302 Aql.

Date	$\Delta\lambda$, nm	V_r, km s^{-1}						
		Emissions		Em/Abs	Absorptions		IS	
		perm.	forb.	Fe II, etc.	Si II+He I	Hα+Hβ	Na I D	DIB
09.08.01	510–670	65	68	36/79	61	68	–	5.6
28.08.04	530–680	67	61	43/83	68	69	11.3	4.8
24.11.07	530–680	65	61	42/77	58	68	11.2	4.5
13.07.08	520–670	65	65	42/79	54	67	11.2	5:
18.08.08	460–600	66	65	45/80	60	70	11.0	5:
3 & 5.11.08	450–590	64	60	46/85	71	72	11.0	4.4
11.09.09	420–880	64	60	39/82	66	69	10.6	3:
31.07.10	440–590	66	59	42/80	60	74	10.8	5:
20.11.10	400–550	64	–	43/80	–	70	–	–
3 & 8.08.12	430–680	65	62	37/81	70	72	10.6	4.4
27.05.13	430–670	64	61	40/81	65	73	10.5	4.8
19.08.13	430–670	66	61	35/80	64	72	10.3	5.2
09.10.13	430–670	66	61	37/82	67	72	10.8	4.6
13.08.14	430–670	66	62	38/83	63	72	11.1	4.2
04.10.14	540–850	65	62	–	65	70	10.5	4:
		Average values of V_r, km s^{-1}						
		65.2	62.0	40.5/80.7	63.7	70.5	10.8	4.6
		±0.3	±0.4	±0.5/0.4	±0.3	±0.4	±0.2	±0.2

The remaining part of the data reduction, including measurements of the lines intensities and positions, was done with the latest version of the DECH20t package [24]. This package, traditionally used in our studies, permits radial velocity measurements for individual features of complex line profiles. Only heliocentric radial velocities, V_r, are used throughout this paper. Their systematic errors do not exceed 1 km s^{-1} for a single line. The latter can be seen in the last column of Table 1, where V_r of the saturated interstellar components of the Na I D–lines are listed. Features in the spectrum of V1302 Aql were identified using an earlier published atlas [25].

3. Results and Discussion

3.1. Spectral type of V1302 Aql in 2001–2014

Earlier spectroscopic observations of V1302 Aql revealed a gradual transition from a normal F–type supergiant [26] to an A5–type one [14]. The new spectral type estimates for 2001–2014 based on our technique presented in [12, 14] give the following results. Pure absorption lines in the blue part of the spectrum indicate a spectral type A6, while inclusion of criteria using He I and Si II absorptions leads to A3.5. Therefore we conclude that the current spectral type coincides with that derived in [12, 14] within the uncertainties and that the objects T_{eff} does not grow anymore.

3.2. Line profiles in the spectrum of V1302 Aql in 2001–2014

As earlier, line profiles in the spectra of V1302 Aql vary from purely absorption with small deviations from symmetry to P Cyg–type profiles and double-peaked emissions. Examples of these line profiles are shown in Fig. 1. Variations of the intensities and profiles for the last 20 years taking into account results from [12, 14, 17] are noticeable but small.

Hydrogen lines Hα and Hβ in 2001–2014 still have a characteristic double-peaked profile, which was observed in the 1990's see Fig. 5 in [14]. Positions of both emission peaks and the central depression have not changed since then. Variations of the residual intensities of the emission components of both lines remained within 40%. The Hα profiles in two spectra are shown in Fig. 2.

A typical peak intensity ratio for the entire 20-year long period is seen in the spectrum taken in 2014. An unusual Hα line profile, when the red peak is significantly stronger than the blue one, is

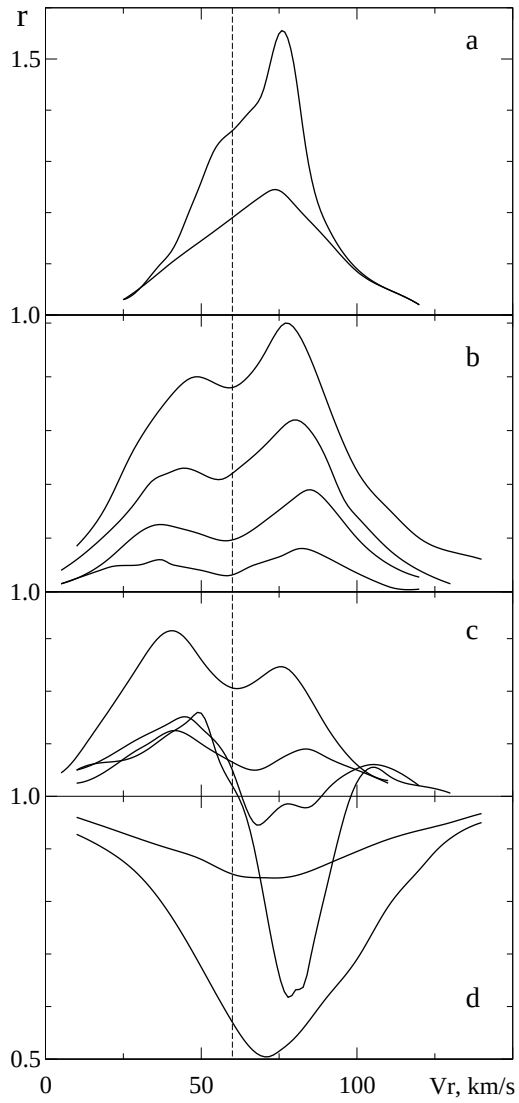

Figure 1. The line profile transformation in the spectra of V1302 Aql in 2012–2014. From top to bottom: a) the forbidden emissions [Fe II] (Multiplet 14F) 7155 Å and [O I] (1F) 6300 Å; b) the emissions Fe II (46) 5991, 6084, and 6113 Å and an average of the Fe I (168) 6394 Å and Ti II (112) 6718 Å; c) the emission Fe II (74) 6417 Å an average of the emissions Cr II (50) 5502 Å and 5511 Å and absorption/emission lines Ti II (69) 5337 Å and Ti II (70) 5154 Å d) the absorptions Si II (5) 5056 Å and Si II (2) 6347 Å. The vertical line shows the systemic velocity $V_{sys} \sim 60\,km\,s^{-1}$ [15].

detected in only one spectrum taken on 2007 November 24. In all other spectra the peak intensity ratio is the opposite [14, 17]. Variations of the residual intensities of the strongest forbidden and permitted Fe II lines are even weaker (within 10%). In the last 7 spectra taken in 2012–2014 they are limited to 20% and 6%, respectively.

3.3. Radial velocities of various features in 2001–2014

According to [15], the average radial velocity of several rotational bands of the CO molecule with respect to the local standard of rest is $V(LSR) = 77\,km\,s^{-1}$. The heliocentric systemic radial velocity of the object is $V_{sys} \sim 60\,km\,s^{-1}$. Humphreys *et al.* [17] determined $V_{sys} = 58 - 60\ km\,s^{-1}$ using a combination of CO and OH bands. We note that the latter is also close to the velocities derived from radio lines of other molecules (see [28] and references therein).

The relative stability of the spectrum of V1302 Aql in recent time and homogeneity of the obtained material allowed us to move from reporting the variety of the spectral line shapes to following a

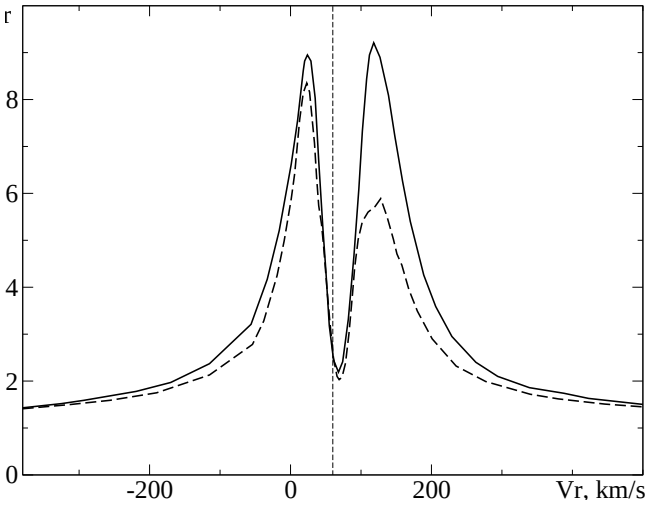

Figure 2. The Hα line profile in the spectra of V1302 Aql in 2007 and 2014. The vertical line shows the systemic velocity $V_{sys} \sim 60$ km s^{-1} [15].

gradual transformation between different shapes. Comparison of Figs. 1 and 3 with the data from Table 1 convinces that such a transformation is real. The profiles shown in Fig. 1 are averaged from the spectra taken in 2012–2014. A typical example of relationships between the radial velocities for individual lines and their residual intensities is shown in Fig. 3. The same profile types follow each other from top to bottom in Fig. 1 and from left to right in Fig. 3 and in Table 1.

Variations of the average radial velocities of various line groups (see Table 1) are small as well. In particular, all the radial velocities for the pure absorptions are in a range of 54–70 km s^{-1}. Forbidden lines are asymmetric (see Fig. 1a), such as the peak intensity is red-shifted with respect to the lower part of the profile by 6 km s^{-1} on average. The [Ca II](1F) 7291 and 7324 Å emissions seen in our spectra taken on 2009 September 11 and 2014 October 4 are much stronger that all other forbidden lines but with no positional shift with respect to the latter. Radial velocities of the entire profiles and their peaks are presented in Fig. 3a by circles and dots, respectively. The averaged radial velocities, measured from lower parts of the forbidden line profiles, are listed in column 3 of Table 1.

Permitted emissions of the iron group are noticeably wider than the forbidden lines. For example, at the same residual intensity of 1.5, the half-widths at the zero level are 70 and 50 km s^{-1}, respectively. The iron lines are clearly double-peaked with a weaker blue-shifted peak (see Fig. 1b). The radial velocities of the lower parts of these emission profiles (in the same way as for the forbidden lines), are shown in column 4 of Table 1 and represented by circles in Fig. 3b. The emission peak velocities are shown by dots in the same Figure. The peak separation decreases from 50 km s^{-1} for weak emissions to 26 km s^{-1} for the strongest ones, where it even reaches a triangular shape. It seems that the double-peaked profiles are not just a sum of two narrower single-peaked emissions separated by 50 km s^{-1}, but that a partially filled absorption component formed in the stellar atmosphere also takes part in the overall profile formation.

It is seen in Figs. 1bc that a gradually deepening absorption "pushes down" the central part of the profile and eventually turns it into an inverse P Cyg–type profile. Line profiles may have this kind of shape in the following cases: when a narrow circumstellar absorption overlaps with a wide circumstellar emission or when two narrower emissions with different radial velocities join together. The inner slopes would be shallower than the outer ones in the latter case. We observe steeper inner slopes instead, therefore the emission components are separated by an absorption. It is possible to have a combination of these two formation mechanisms as well as a double–ray version suggested in [10].

There a many lines with emission components on both sides of the absorption in the spectrum of V1302 Aql. We include in the group of lines with an inverse P Cyg–profile those with the continuum above the absorption core, $r < 1$. If the central depression is seen at $r > 1$, the line is considered to have a double-peaked profile. Column 5 of Table 1 contains the average radial velocities for blue-shifted

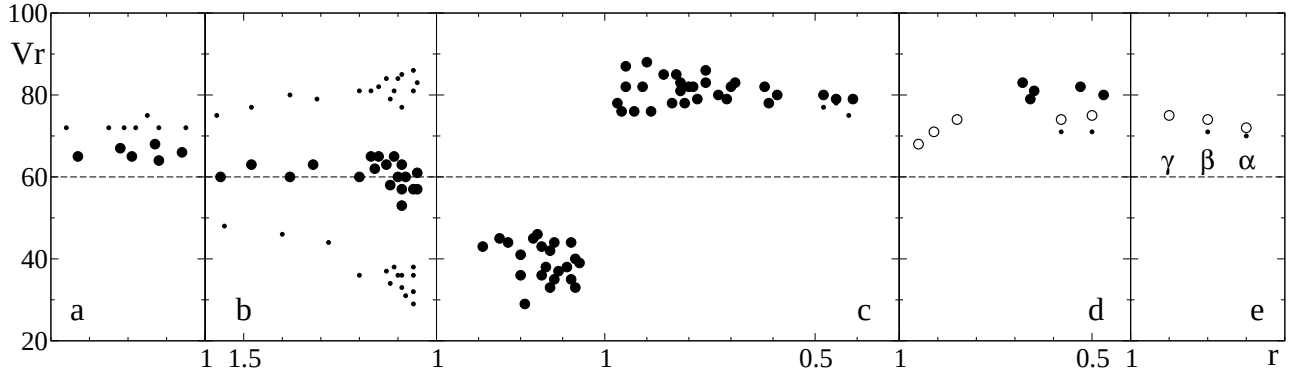

Figure 3. The relationships between the heliocentric radial velocities and residual intensities of the line components in the spectra of V1302 Aql on 2008 August 3 and 8. The horizontal dashed line shows the systemic velocity $V_{sys} \sim 60\,km\,s^{-1}$ [15]. a) Forbidden emissions (whole profiles are shown by filled circles, while their peaks are shown by dots). b) Permitted double-peaked profiles (symbols are the same as in part a). c) Lines with inverse P Cyg–profiles (emission and absorption components are shown by filled circles, while cores of the strongest absorptions are shown by dots). d) Fe II absorptions (whole profiles are shown by circles) and He I and Si II absorptions (whole profiles are shown by open circles, cores are shown by dots). e) Absorption components of the H I lines (symbols are the same as in part d).

emission and absorption components in the group of lines with P Cyg–profiles. Both such components are shown by circles in Fig. 3c (an absorption asymmetry is shown for the strongest ones). The red-shifted components are weaker (r <1.1) than the blue-shifted ones with an average radial velocity of $130\pm10\,km\,s^{-1}$ in our spectra.

The profiles in Fig. 1 differ from classic P Cyg–profiles which represent a spherically-symmetric envelope with a radial velocity gradient. The latter show a relationship between the emission component intensity and the absorption component depth. However the weakest absorptions in our profiles (r <0.95) may be accompanied by blue-shifted emissions with any intensity in a range $1.0 < r < 1.4$, while the strongest absorptions (r ∼0.4) are seen with the weakest ones (r <0.15). This is seen in Fig. 3 where the leftmost filled circles of the lower chain correspond to the leftmost (not the rightmost!) circles of the upper chain.

The line profiles that are totally located below the continuum make the group of absorptions. However, some of these lines, such as Fe II (37,38), Ti II (31), Cr II, may have hidden outside emission components, because their wings are narrower than those of Si II and Mg II with similar depths. Fig. 3d shows the uncertain absorption group members by filled circles, while more reliable ones are shown by open circles. In turn, we consider the most pure absorptions are the weakest ones, such as Si II (4,5) and He I 5876 Å (the left subgroup of the open circles in Fig. 3d). The average radial velocities for the latter lines are given in column 6 of Table 1. A standard deviation for the pure absorption and emissions is $\sigma \leq 0.4$ km s^{-1} and $\sigma = 0.2$ km s^{-1} for the interstellar features.

Closeness of the radial velocities seen in Fig. 3 is noticeable in the following line groups:

– iron absorption lines in the blue part of the spectrum and absorption components of the lines with inverse P Cyg–profiles (averaging all our data gives 81 and 80 km s^{-1}, respectively). We consider stable positions of the latter as an indicator of a matter infall;

– strong Si II (2) absorptions (they are shown by a pair of open circles in Fig. 3d) and absorption components of the Hα and Hβ lines (average radial velocities are 73 and ∼70 km s^{-1}, respectively);

– the weakest absorptions and forbidden emissions (63.7 and 65.2 km s^{-1}, respectively). Since the former form in the deepest layers of the photosphere (or pseudo-photosphere) while the latter form in an extended envelope, it is natural that the radial velocity of the latter is the closest to that of the star's center of mass, i.e. $V_{sys} \sim 60\,km\,s^{-1}$.

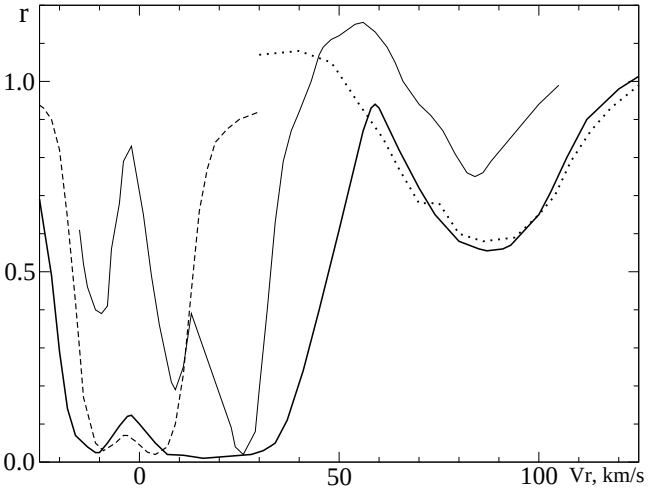

Figure 4. The Na I D1 line profile in the spectra of V1302 Aql (thick solid line) and HD 183143 (dashed line). The thin solid line shows the profile of the K I (1) 7665 Å line in the spectrum of V1302 Aql. The dotted line shows the Fe II 5316 Å line profile in the spectrum of V1302 Aql. Spectra of both stars were taken with the same spectrograph NES.

4. Interstellar features in the spectrum of V1302 Aql

Fig. 4 shows a complex profile of the D1–line of a resonance Na I doublet. The mail part of its absorption component forms in a cold interstellar gas in the line of sight, while a weaker red-shifted component forms in the atmosphere of V1302 Aql. The latter is well reproduced by the absorption component of the Fe II 5316 Å line, and both can apparently be classified as lines with inverse P Cyg–profiles.

The main part of the Na I D–line profile in a range of $V_r = -25 - +50\,km\,s^{-1}$ has interstellar nature. As follows from a recent compilation of the data on the structure and kinematics of the Milky Way [27], radial velocity in the direction of V1302 Aql increases with distance and reaches $+50\,km\,s^{-1}$ at a distance D = 5.3 kpc. Fig. 4 shows the Na I D1–line profile in the spectrum of the B–type hypergiant HD 183143, which is projectionally close to V1302 Aql (the Galactic coordinates $l/b = 53.^{\circ}2/0.^{\circ}6$ and $47.^{\circ}1/-2.^{\circ}5$, respectively). However, as seen in Fig. 1 in [28], HD 183143 is located between the local and Carina–Norma spiral arms, while the line of sight to V1302 Aql passes through the latter arm between 3 and 8 kpc. Therefore, a distance toward HD 183143 is ∼2 kpc [29], and V1302 Aql is located significantly further away. Coincidence of the red boundary of the interstellar Na I absorption and the maximum of above mentioned V_r(D) relationship indicates that V1302 Aql cannot be closer than 5.3 kpc. Its spectroscopic parallax moves it even further away to 6.5–8.0 kpc.

The K I 7665 Å line profile shown in Fig. 4 also represents a combination of stellar and interstellar components. The interstellar components are less saturated compared to those of the Na I D–lines and split into three components. The weakest of them at $V_r \sim -10\,km\,s^{-1}$ corresponds to the blue-shifted component of the Na I D1 line (Fig. 4), while the other two at $V_r \sim 8$ and $24\,km\,s^{-1}$ are merged in the Na I profile. The stellar absorption component is located at $V_r \sim 84\ km\,s^{-1}$. As clearly seen in Fig. 4, the K I 7665 Å line profile also has an emission component, whose position at $V_r \sim 84\,km\,s^{-1}$ indicates that it forms in the circumstellar envelope.

Using our large high-quality material, we measured positions of some diffuse interstellar band (DIB). A list of those reliably identifiable in the spectrum of V1302 Aql was published in [25]. Note two important points concerning the search and measurement of the DIB positions:

– the number of DIBs with measured V_r varies from one spectrum to another (from 5 to 17 features);

– the individual DIBs V_r differ systematically.

The latter was mentioned by Oudmaijer [16], who has identified many DIBs in the object's spectrum. Over 30 of them are narrow and have equivalent widths of ≥20 mÅ. The author explained a large scatter of the measured V_r (from 5 to $40\,km\,s^{-1}$) by uncertain DIB wavelengths.

The last column of Table 1 lists average V_r for each of the observing dates in 2001–2014 of a small group of the narrowest and most symmetric DIBs which show the smallest differential shifts. Their standard wavelengths (5796.97, 5849.82, 6195.96, 6376.00, and 6379.24 Å) are taken from [30]. After such a selection, the average V_r for all the dates came to $4.6\pm0.2\,\mathrm{km\,s^{-1}}$.

5. Closest analogs of the hypergiant V1302 Aql

In Sect. 1 we mentioned ρ Cas, a well-studied yellow hypergiant with a luminosity similar to that of V1302 Aql. In particular, optical spectra of ρ Cas and a complex structure of its atmosphere and envelope have been recently studied in detail [7, 31]. However if all features are taken into account, the optical counterpart of the IR-source IRAS 18357−0604 turns out to be closer to V1302 Aql. Since this object is very reddened, not much data have been published for it. Recently authors [32] took a spectrum of IRAS 18357−0604 in the red and IR regions, estimated its distance $D\sim6$ kpc using its systemic velocity, classified it an early A–type star, and concluded on a similarity of its spectrum to that of V1302 Aql. The spectrum of IRAS 18357−0604 is dominated by asymmetric emissions of low-excitation transitions, such as H I, N I, Fe I, Fe II, Ti II, [Fe II], etc. According to these authors, line profile features of IRAS 18357−0604 indicate an asymmetry of its outflowing envelope. However unlike in the spectrum of V1302 Aql, red-shifted components of broad double-peaked profiles of H I, Ca II, and N I in the spectrum of IRAS 18357−0604 are stronger than blue-shifted ones.

A bright star HR 8752, the optical counterpart of the IR source IRAS 22579+5640, is also a member of the yellow hypergiants group. It is located much closer to the Sun compared to V1302 Aql, and it is easier to study its features. HR 8752 is listed as a standard of MK–classification with a spectral type G0 Ia [33]. However comparing high-resolution spectra taken in 1973–1977, authors [34] have detected a growth of its $T_{\rm eff}$. The same authors studied kinematic properties of the star's atmosphere and envelope in detail and noted signs of a matter infall onto the star with a speed of 30 $\mathrm{km\,s^{-1}}$. Later, based on a set of optical spectra of HR 8752 obtained with various instruments in 1973–2005, Nieuwenhuijzen *et al.* [35] have analysed these data using a homogeneous approach. Adding data from even a longer photometric monitoring, they restored temporal variations of the star's fundamental parameters, such as $T_{\rm eff}$, luminosity, radius, color-index $B-V$, etc. One of their main results is a conclusion about a gradual growth of $T_{\rm eff}$ from $\log T_{\rm eff}=3.65$ circa 1900 to $\log T_{\rm eff}=3.90$ in 2000. Therefore, HR 8752 is the closest analog of V1302 Aql based on all features. At the same time, HR 8752 seems to have a lower mass compared to that of V1302 Aql judging on the HRD position [35].

Comparison of the spectral line profiles in our spectra of V1302 Aql in 2001–2014 indicates the absence of a noticeable spectral variability, thus allowing to conclude that the hypergiant entered a phase of a slow down (or termination) of the $T_{\rm eff}$ growth and approached the Yellow Void boundary, which is called the White Wall [10]. Earlier authors [36] suspected stabilization of the star's $T_{\rm eff}$ based on a long-term photometric monitoring. New evolutionary loops may follow this episode, such as that observed for HR 8752 on a timescale of 10 years [18]. Therefore, it seems very important to continue monitoring of V1302 Aql.

6. Conclusions

Using a set of high-resolution spectra of V1302 Aql obtained in 2001–2014, we measured intensities and positions of various spectral features that allowed us to analyse the profile behaviour with time as well as the velocity field in various layers of the object's extended atmosphere and its circumstellar envelope. We concluded on a closeness of the V_r for the iron absorption lines in the blue spectral part and absorption components with inverse P Cyg–profiles. Positions of the latter features that reflects clumps falling onto the star with a velocity of $\sim20\,\mathrm{km\,s^{-1}}$ has been stable for all the observing dates. The position of the strong Si II (2) absorptions and absorption components of the Hα and Hβ lines varied insignificantly around 63.7 and 70.5 $\mathrm{km\,s^{-1}}$, respectively.

The V_r for the weakest absorptions, which form in the deepest observable photospheric (or pseudo-photospheric) layers, and for the forbidden emissions, which form in an extended envelope (63.7 and 65.2 $\mathrm{km\,s^{-1}}$, respectively). The average V_r of the permitted emissions also weakly deviates from that

of the pure absorptions. It is equal to 62.0 km s^{-1} for all the observing dates. The average V_r of the interstellar features is equal to 4.6±0.2 km s^{-1}.

Comparison of the features in the spectra of V1302 Aql in 2001–2014 indicates the absence of a noticeable variability. We conclude that the hypergiant entered a phase of a slow down (or termination) of the T_{eff} growth and approached the high-temperature boundary of the Yellow Void.

Acknowledgments

This study was accomplished with a financial support of the Russian Foundation for Basic Research (RFBR) in the framework of the project No.14–02–00291 a. A.M. acknowledges support of his travel to the McDonald Observatory from the Department of Physics and Astronomy of the University of North Carolina at Greensboro. We have made use of the astronomical data bases SIMBAD and ADS.

References

1. Hrivnak B.J., Kwok S., Volk K.M., 1989, Astrophys. J. **346** 265

3. Jones T.J., Humphreys R.M., Gehrz R.D., 1993, Astrophys. J. **411** 323

2. Blöcker T., 1995, Astron and Astrophys. **299** 755

4. de Jager C., 1998, Ann. Rev. Astron. Astrophys. **8** 145

5. de Jager C., Lobel A., Nieuwenhuijzen H, Stothers R., 2001, Mon. Not. R. Astron. Soc. **327** 452

6. Oudmaijer R.D., Davies B., de Wit W.-J., Patel M., 2009, ASP Conf. Series, eds. D.G. Luttermoser, B.J. Smith, and R.E. Stencel, **412** 17

7. Klochkova, V.G., Panchuk, V.E., Tavolganskaya, N.S., Usenko, I.A., 2014, Astron. Rep. **58** 101

8. Schuster M.T., Humphreys R.M., Marengo M., 2006, Astron. J. **131** 603

9. Driebe T., Groh J.H., Hofmann K.-H., *et al.*, 2009, Astron and Astrophys. **507** 301

10. Oudmaijer R.D., de Wit W.-J., 2013, Astron and Astrophys. **551** A69

11. Meynet G., Maeder A., 2003, Astron and Astrophys. **404** 975

12. Klochkova V.G., Chentsov E.L., Panchuk V.E., 1997, Mon. Not. R. Astron. Soc. **292** 19

13. Miroshnichenko A., Danford S., Verdugo E., *et al.*, 2013, In: Massive Stars: From α to Ω, held 10–14 June 2013 in Rhodes, Greece, Online at http://a2omega-conference.net, id.169

14. Klochkova V.G., Yushkin M.V., Chentsov E.L., Panchuk V.E., 2002, Astron. Rep. **46** 139

15. Oudmaijer R.D., Groenewegen M.A.T., Matthews H.E., *et al.*, 1996, Mon. Not. R. Astron. Soc. **280** 1062

16. Oudmaijer R.D., 1998, Astron and Astrophys. Suppl. **129** 541

17. Humphreys R.M., Davidson K., Smith N., 2002, Astron. J. **124** 1026

18. de Jager C., Nieuwenhuijzen H., 1997, Mon. Not. R. Astron. Soc. **290** 50

19. Panchuk V.E., Yushkin M.V., Najdenov I.D., 2003, Preprint Spec. Astrophys. Obs., No. 179

20. Panchuk V.E., Klochkova V.G., Yushkin M.V., Najdenov I.D., 2009, Journal of Optical Technology **76** 87

21. Panchuk V.E., Klochkova V.G., Galazutdinov G.A., *et al.*, 1993, Astronomy Letters **19** 431

22. Yushkin M.V., Klochkova V.G., 2005, Preprint Spec. Astrophys. Obs., No. 206

23. Tull R.G., MacQueen P.J., Sneden C., Lambert D.L, 1995, Publ. Astron. Soc. Pasif. **107** 251

24. Galazutdinov G.A., 1992, Preprint Spec. Astrophys. Obs., No. 192

25. Chentsov E.L., Klochkova V.G., Tavolganskaya N.S., 1999 Bull. Spec. Astrophys. Obs. **48** 25

26. Humphreys R.M., Strecker D.W., Murdock T.L., Low F.J., 1973, Astrophys. J. **179** 49

27. Reid M.J., Menten K.M., Brunthaler A., *et al.*, 2014, Astrophys. J. **783** 130

28. Quintana-Lacaci G., Agúndez M., Cernicharo J., *et al.*, 2013 Astron and Astrophys. **560** L2

29. Chentsov E.L., 2004, Astronomy Letters **30** 325
30. Weselak T., Galazutdinov G.A., Inwoo H., Krelowski H., 2010, Mon. Not. R. Astron. Soc. **401** 1308
31. Gorlova N., Lobel A., Burgasser A.J., *et al.*, 2006, Astrophys. J. **651** 1130
32. Clark J.S., Negueruela I., González-Fernández C., 2014, Astron and Astrophys. **561** A15
33. Morgan W.W., Roman N.G., 1950, Astrophys. J. **112** 362
34. Lambert D.L., Luck R.E., 1978, Mon. Not. R. Astron. Soc. **184** 405
35. Nieuwenhuijzen H., de Jager C., Kolka I., *et al.*, 2012, Astron and Astrophys. **546** A105
36. Patel M., Oudmaijer R.D., Vink J.S., *et al.*, 2008, Mon. Not. R. Astron. Soc. **385** 967